Journal of Power Sources 180 (2008) 648–652

Contents lists available at ScienceDirect

Journal of Power Sources

journal homepage: www.elsevier.com/locate/jpowsour

Short communication

Effects of addition of manganese and $LmNi_{4.1}Al_{0.25}Mn_{0.3}Co_{0.65}$ alloy on electrochemical characteristics of $Ti_{0.32}Cr_{0.43-x}Mn_xV_{0.25}$ ($x = 0$–0.08) alloys as anode materials for nickel–metal-hydride batteries

Jong-Yun Kim [a], Choong-Nyeon Park [a], Jong-Su Shim [a], Chan-Jin Park [a,*], Jeon Choi [b], Hak Noh [c]

[a] Department of Materials Science and Engineering, Chonnam National University, 300, Yongbong-dong, Buk-gu, Gwangju 500-757, Republic of Korea
[b] Department of Advanced Materials Engineering, Hanlyo University, 199-4, Dokryeri, Kwangyang, Chonnam 545-704, Republic of Korea
[c] Technical Research Center, Alphadent Co. Ltd., 371-37 Gasan-dong, Geumcheon-gu, Seoul 158-302, Republic of Korea

ARTICLE INFO

Article history:
Received 5 October 2007
Received in revised form 12 December 2007
Accepted 22 January 2008
Available online 26 February 2008

Keywords:
Ti–Cr–V alloy
Nickel–metal-hydride battery
Ball-milling
Manganese substitution
Activation
Discharge capacity

ABSTRACT

This study examines the effects of the addition of Mn and $LmNi_{4.1}Al_{0.25}Mn_{0.3}Co_{0.65}$ (Lm: lanthanum-rich mischmetal) alloy on the electrochemical characteristics of body centered cubic (BCC) type $Ti_{0.32}Cr_{0.43-x}Mn_xV_{0.25}$ ($x = 0$–0.08) alloys as negative electrode (anode) materials for nickel–metal-hydride (Ni-MH) batteries. The activation behaviour and discharge capacity of the BCC alloys are improved significantly by ball-milling with $LmNi_{4.1}Al_{0.25}Mn_{0.3}Co_{0.65}$ alloy because this AB_5 alloy acts as a path for hydrogen on the surface of the BCC alloy. Among the Mn-substituted alloys, a $Ti_{0.32}Cr_{0.38}Mn_{0.05}V_{0.25}$ alloy ball-milled with the AB_5 alloy yields the greatest discharge capacity of 340 mAh g^{-1}. In addition, compared with the alloy without Mn, the Mn-substituted alloys exhibit a lower plateau pressure for hydrogen, a better hydrogen-storage capacity in the pressure–composition isotherms and faster surface activation.

1. Introduction

The hybrid electric vehicle (HEV) uses both an internal combustion engine and a secondary battery, and has considerably better fuel economy than conventional internal combustion engines. Recently, the HEV has become increasingly popular due to the recent high price of oil. Consequently, there is increased demand for nickel–metal-hydride (Ni-MH) secondary batteries for HEVS. In addition, the market for industrial, high capacity, secondary batteries is rapidly changing from traditional lead-acid or nickel–cadmium batteries to the environmentally friendly Ni-MH battery.

$LaNi_5$ (AB_5) hydrogen-storage alloys are currently used as negative electrode (anode) materials for Ni-MH batteries. There have, however, been continuous efforts to enhance the electrode characteristics of AB_5 alloys and to use new, high-performance versions for anode materials [1–16].

Body centered cubic (BCC) Ti or V based alloys have an effective hydrogen-storage capacity of more than 2 wt.%, and show a proper plateau pressure in the pressure–composition (P–C) isotherm curve for the absorption and desorption of hydrogen, which is suitable for their use as an anode material in Ni-MH batteries [17–21]. Nevertheless, BCC type Ti or V based alloys are barely activated during charging due to the formation of a dense oxide film on the alloys in an alkaline solution, and have a low catalytic activity for the charge-transfer reaction [21,22]. Consequently, the discharge capacity of these alloys is generally much lower than the respective theoretical values. Thus, further improvement in the discharge capacity of the alloys is needed for their practical application in Ni-MH batteries. Tsukahara et al. [23–25] recently reported that the electrode characteristics of V-based solid-solution alloys could be significantly improved by the formation of a TiNi network as a catalyst and/or current-collector in the alloys.

The aim of this study is to improve the discharge capacity and surface activation of $Ti_{0.32}Cr_{0.43}V_{0.25}$ alloys of the BCC type by substituting Mn for Cr and ball-milling with the more active $LmNi_{4.1}Al_{0.25}Mn_{0.3}Co_{0.65}$ (Lm: lanthanum-rich mischmetal) AB_5 type alloy.

2. Experimental

Based on the composition of $Ti_{0.32}Cr_{0.43}V_{0.25}$, Mn was partially substituted for Cr in the alloy. The compositions of the Mn-substituted alloys used in the study were $Ti_{0.32}Cr_{0.4}Mn_{0.03}V_{0.25}$,

* Corresponding author. Tel.: +82 62 530 1704; fax: +82 62 530 1699.
E-mail address: parkcj@chonnam.ac.kr (C.-J. Park).

0378-7753/$ – see front matter © 2008 Elsevier B.V. All rights reserved.
doi:10.1016/j.jpowsour.2008.01.098

$Ti_{0.32}Cr_{0.38}Mn_{0.05}V_{0.25}$ and $Ti_{0.32}Cr_{0.35}Mn_{0.08}V_{0.25}$. An AB_5 type alloy of $LmNi_{4.1}Al_{0.25}Mn_{0.3}Co_{0.65}$ was also used for ball-milling with the Ti–Cr–V alloys. Each alloy was melted in a vacuum arc furnace and prepared as a 40 g ingot. The alloys were then crushed to a 100–325 mesh powder.

A mixture of the BCC and AB_5 alloy powders was ball-milled for 20 min in a mode of '8' type rotation. A 65 cm^3 stainless steel jar and 7/32 in. stainless balls were used in the ball-milling process. The ratio of the mixed alloy powder to crush balls and the AB_5 to BCC alloy ratio in the mixed powder was 1:14 and 1:5, respectively. All processes for ball-milling were carried out in an inert argon atmosphere.

The pressure–composition (*P*–*C*) isotherms were measured at 303 K using approximately 1 g of the powder, which had with a particle size ranging from 100 to 300 μm, in a Sivert type hydrogen reactor. In addition, X-ray diffraction (XRD), scanning electron microscopy (SEM) and energy dispersive spectroscopy were used to observe the structure, morphology and chemical composition of the alloys, respectively.

Paste-type electrodes were fabricated by mixing the alloy powder, hydroxyl propyl methyl cellulose (HPMC), a 503H binder and carbon black, and then pasting the resultant slurry on to a foamed nickel gauze. The resulting coated gauze was then dried and cut into 20 mm × 20 mm sections.

Electrochemical measurements were carried out using a cell that consisted of an alloy electrode, a Pt counter electrode and an Hg/HgO reference electrode in a 6 M KOH electrolyte. The hydrogen-storage capacity of the BCC Ti-based alloys was approximately 2 wt.%, which corresponds to 500 mAh g^{-1} for the electrode. Therefore, the electrodes were charged for 10 h at 50 mA, and were maintained for 5 min in an open-circuit condition after each charging and discharging step. The cut-off voltage for discharge was −650 mV versus Hg/HgO.

The potentiodynamic polarization tests were carried out at a scan rate of 1 mV s^{-1} to determine the effects of Mn substitution for Cr on the chemical stability of the alloy. In addition, the electrochemical impedance spectrum (EIS) of the alloys was analyzed.

3. Results and discussion

3.1. Effect of ball-milling on crystal structure of alloy powders

Fig. 1 shows the XRD patterns for the $Ti_{0.32}Cr_{0.43-x}Mn_xV_{0.25}$ (x = 0.03–0.08) alloys, where Mn is partially substituted for Cr, and for the $LmNi_{4.1}Al_{0.25}Mn_{0.3}Co_{0.65}$ alloy before and after ball-milling. Before ball-milling, the former (BCC) alloys and the latter (AB_5) alloy show a BCC and a $CaCu_5$ structure, respectively. By contrast, peaks corresponding to the AB_5 alloy in the XRD patterns of the BCC and AB_5 type alloy mixture disappear after ball-milling. The significant weakening of the peaks corresponding to $LmNi_{4.1}Al_{0.25}Mn_{0.3}Co_{0.65}$ alloy suggests that its particles become ultrafine by ball-milling for 20 min. In our previous work [26], the calculated average particle size of $LmNi_{4.1}Al_{0.25}Mn_{0.3}Co_{0.65}$ alloy in a mixture of $Ti_{0.32}Cr_{0.43}V_{0.25}$ alloy and $LmNi_{4.1}Al_{0.25}Mn_{0.3}Co_{0.65}$ alloy after ball-milling for 20 min was about 15 nm.

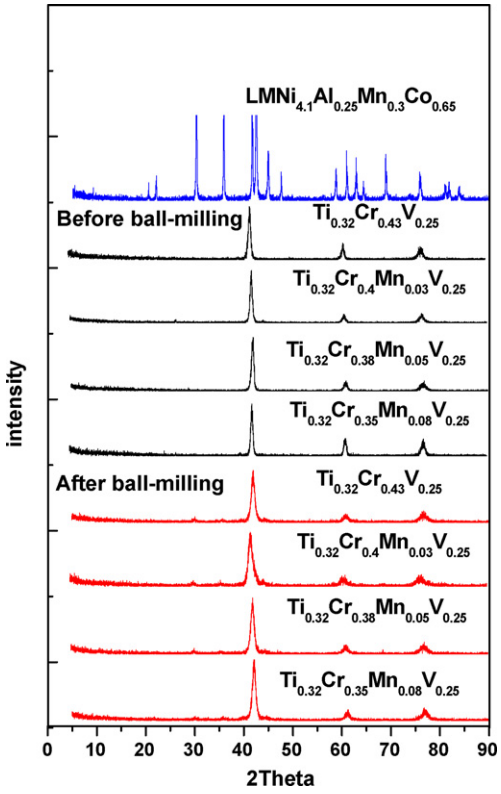

Fig. 1. XRD patterns of $Ti_{0.32}Cr_{0.43-x}Mn_xV_{0.25}$ (x = 0–0.08) alloys and $LmNi_{4.1}Al_{0.25}Mn_{0.3}Co_{0.65}$ alloy before and after ball-milling.

3.2. Effect of ball-milling on surface morphology of the mixed alloy powder

Fig. 2 shows the back-scattered electron (BSE) image and EDS spectrum of the surface of the mixed powder of $Ti_{0.32}Cr_{0.43}V_{0.25}$ and $LmNi_{4.1}Al_{0.25}Mn_{0.3}Co_{0.65}$ alloys after ball-milling. From EDS analysis, the bright (A) and dark areas (B) corresponds to the AB_5 and the BCC alloy, respectively. This suggests that the AB_5 alloy exists on part of the surface of the BCC alloy after ball-milling. The AB_5 alloy layer on the surface of the BCC alloy may act as a path for the absorption and desorption of hydrogen, and contribute to improving the surface activation of the electrode.

3.3. Effect of Mn on absorption and desorption of hydrogen

Pressure–composition (*P*–*C*) isotherms of the BCC $Ti_{0.32}Cr_{0.43-x}Mn_xV_{0.25}$ (x = 0.3–0.8) and AB_5 $LmNi_{4.1}Al_{0.25}Mn_{0.3}Co_{0.65}$ alloys before ball-milling are presented in Fig. 3. The maximum and effective hydrogen capacity are defined as the amount of hydrogen adsorbed at a hydrogen pressure of 5.0 MPa and the amount of hydrogen desorbed from 5.0 to 0.02 MPa, respectively. In addition, the theoretical discharge capacity is calculated using

Table 1
Maximum and effective hydrogen capacity and theoretical discharge capacity of $Ti_{0.32}Cr_{0.43-x}Mn_xV_{0.25}$ (x = 0–0.08) and $LmNi_{4.1}Al_{0.25}Mn_{0.3}Co_{0.65}$ alloys

Alloy	$(H/M)_{max}$ (wt.%)	$(H/M)_{eff}$ (wt.%)	Theoretical discharge capacity (mAh g^{-1})
$Ti_{0.32}Cr_{0.43}V_{0.25}$	3.11	1.82	489
$Ti_{0.32}Cr_{0.4}Mn_{0.03}V_{0.25}$	3.46	1.85	493
$Ti_{0.32}Cr_{0.38}Mn_{0.05}V_{0.25}$	3.47	2.26	606
$Ti_{0.32}Cr_{0.35}Mn_{0.08}V_{0.25}$	3.32	2.00	537
$LmNi_{4.1}Al_{0.25}Mn_{0.3}Co_{0.65}$	2.65	1.01	367

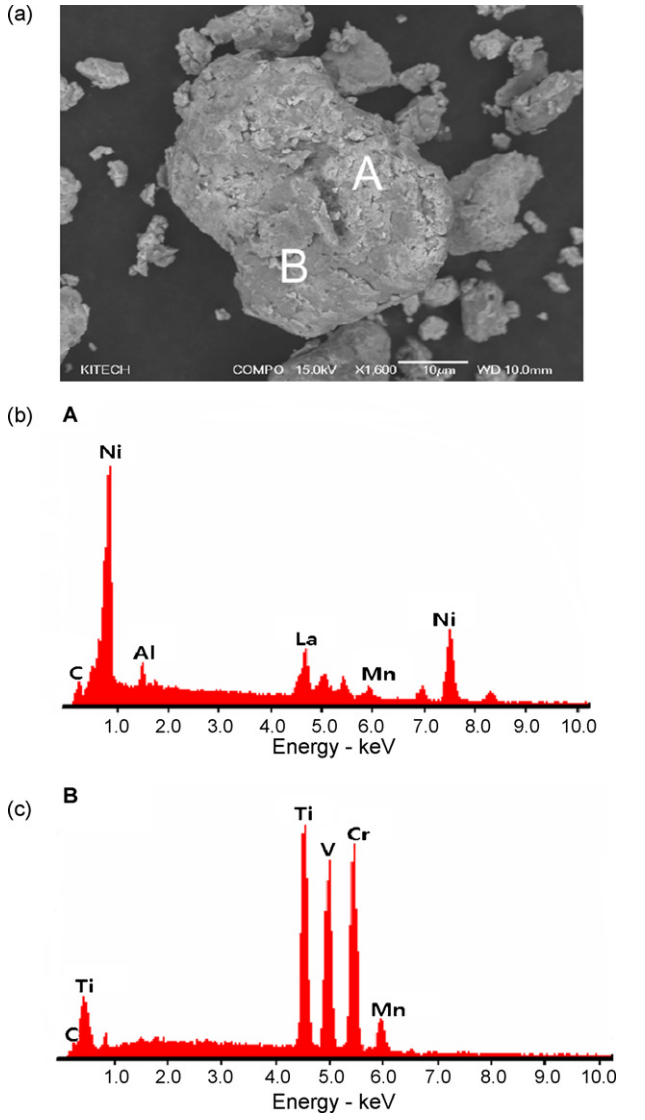

Fig. 2. BSE images and EDS spectra of surfaces of mixed powders of $Ti_{0.32}Cr_{0.43}V_{0.25}$ and $LmNi_{4.1}Al_{0.25}Mn_{0.3}Co_{0.65}$ alloys after ball-milling for 20 min.

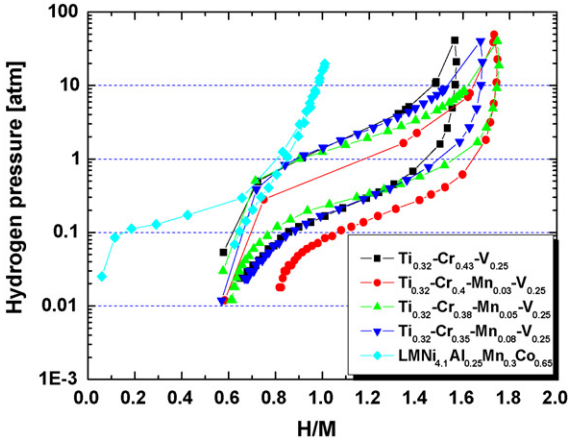

Fig. 3. *P–C* isotherms of $Ti_{0.32}Cr_{0.43-x}Mn_xV_{0.25}$ (x = 0–0.08) alloys and $LmNi_{4.1}Al_{0.25}Mn_{0.3}Co_{0.65}$ alloy.

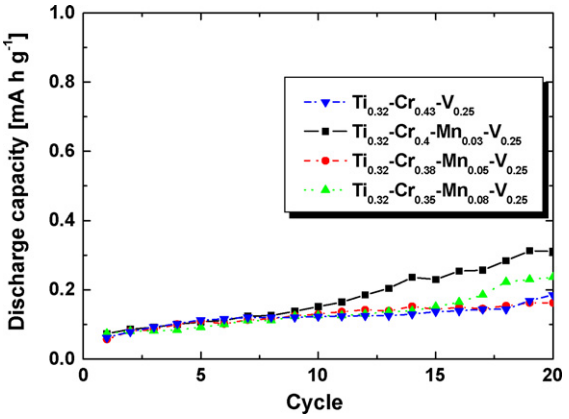

Fig. 4. Effect of addition of Mn on discharge capacity of $Ti_{0.32}Cr_{0.43-x}Mn_xV_{0.25}$ (x = 0–0.08) alloys.

Eq. (1) [27]:

$$C_{th} = \frac{F(\text{wt.\%})}{360} \quad (\text{mAh g}^{-1}) \tag{1}$$

where C_{th} is the theoretical discharge capacity, F the Faraday constant and wt.% is the effective hydrogen capacity. The results are listed in Table 1. The actual discharge capacity of the alloy is generally lower than the theoretical value.

For the Mn-substituted alloys, the plateau pressure is lower and the effective hydrogen capacity is higher than the $Ti_{0.32}Cr_{0.43}V_{0.25}$ alloy without Mn. This suggests that the absorption and desorption of hydrogen in the alloys becomes easier on the addition of Mn.

3.4. Effect of addition of Mn and AB_5 type alloy on discharge capacity of alloy electrodes

The discharge capacities of the BCC $Ti_{0.32}Cr_{0.43-x}Mn_xV_{0.25}$ (x = 0–0.08) alloys are given in Fig. 4. The alloys deliver a much lower discharge capacity than the theoretical values presented in Table 1. This is because a Ti- or V-rich oxide can be formed on the surface of BCC alloys, which can inhibit the absorption of hydrogen during charging [21,22].

The discharge capacity of the BCC $Ti_{0.32}Cr_{0.43-x}Mn_xV_{0.25}$ (x = 0–0.08) alloys ball-milled with 20 wt.% AB_5 $LmNi_{4.1}Al_{0.25}Mn_{0.3}$ alloy are shown in Fig. 5. The capacity increases significantly by ball-milling with the AB_5 alloy. Furthermore, among the Mn-substituted alloys, the $Ti_{0.32}Cr_{0.38}Mn_{0.05}V_{0.25}$ alloy exhibits the greatest dis-

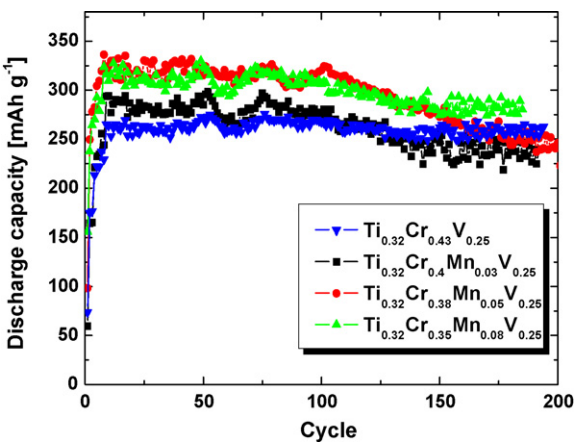

Fig. 5. Effect of addition of Mn and $LmNi_{4.1}Al_{0.25}Mn_{0.3}Co_{0.65}$ alloy on discharge capacity of $Ti_{0.32}Cr_{0.43-x}Mn_xV_{0.25}$ (x = 0–0.08) alloys.

charge capacity of 340 mAh g^{-1}. This suggests that the surface of the BCC alloys can be activated easily by ball-milling, whereby AB_5 alloy particles are embedded in the BCC alloys and act as a path for hydrogen penetration. Furthermore, for the Mn-substituted alloys, the discharge capacity is larger and the activation is faster than for the $Ti_{0.32}Cr_{0.43}V_{0.25}$ alloy. This also suggests that Mn can facilitate surface activation of the alloy by inducing pulverization of the alloy particles. Nevertheless, the Mn-substituted alloys, in which the more active Mn partially substitutes for the Cr (which enhances corrosion resistance of the alloy), give a poorer cycle-life than the $Ti_{0.32}Cr_{0.43}V_{0.25}$ alloy.

3.5. Effect of Mn and AB_5 type alloy on electrochemical characteristics of alloys

Fig. 6 shows the influence of Mn substitution and ball-milling with the AB_5 $LmNi_{4.1}Al_{0.25}Mn_{0.3}$ alloy on the electrochemical impedance plots for the $Ti_{0.32}Cr_{0.43-x}Mn_xV_{0.25}$ (x = 0–0.08) alloys. The AB_5 $LmNi_{4.1}Al_{0.25}Mn_{0.3}$ alloy exhibits the smallest semicircle, while the BCC $Ti_{0.32}Cr_{0.43}V_{0.25}$ alloy gives the largest. The diameter of the semicircle measured from the impedance plot represents the charge-transfer resistance (R_{ct}) of the electrode. The smaller R_{ct} reflects an easier electrochemical charge-transfer reaction on the electrode surface. The electrochemical activation of the BCC $Ti_{0.32}Cr_{0.43}V_{0.25}$ alloy barely proceeds because a Ti or V oxide layer can form on the alloy and inhibits hydrogen absorption through the surface [21,22]. For the Mn-substituted alloys, the magnitude of the impedance follows in the order of Mn content (0.05%, 0.03% and 0.08%). This is also coincident with the fact that the discharge capacity of the Mn-substituted alloys is larger than that of the $Ti_{0.32}Cr_{0.43}V_{0.25}$ alloy.

Potentiodynamic curves of the $Ti_{0.32}Cr_{0.43-x}Mn_xV_{0.25}$ alloys are presented in Fig. 7. Generally, in the potentiodynamic curve for a passive metal, a lower passive current density indicates that the passive film provides better protection of the alloy and higher corrosion resistance. The passive current for the alloys containing 0.03%, 0.05% and 0.08% Mn is higher than for the alloy without Mn. This suggests that the passive film on a Mn-substituted alloy is less stable than that of the alloy without Mn, and the Mn-substituted alloys can be activated easily. However, it also indicates that the Mn-substituted alloys have poorer corrosion resistance and lower cycle-life when used as an electrode for a long period of time. This hypothesis is confirmed by the observation that the Mn-substituted alloys have a poorer cycle-life than the alloy without Mn, as shown in Fig. 5.

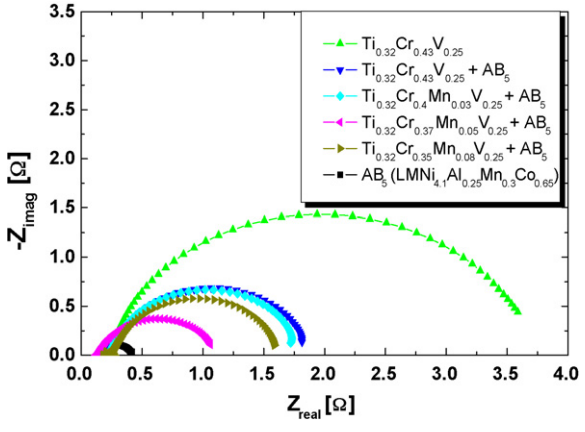

Fig. 6. Effect of addition of Mn and $LmNi_{4.1}Al_{0.25}Mn_{0.3}Co_{0.65}$ alloy on electrochemical impedance plots of $Ti_{0.32}Cr_{0.43-x}Mn_xV_{0.32}$ (x = 0–0.08) alloys.

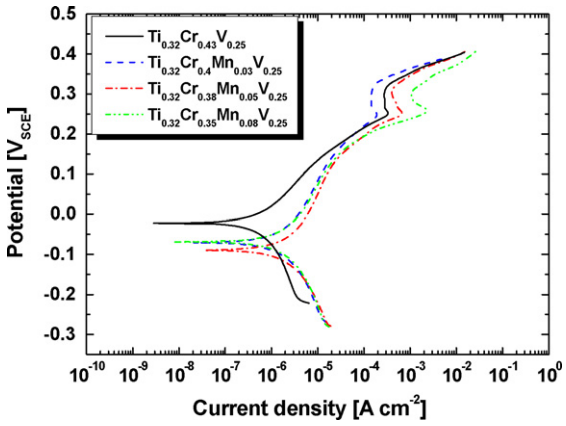

Fig. 7. Effect of Mn on potentiodynamic curves of $Ti_{0.32}Cr_{0.43-x}Mn_xV_{0.25}$ (x = 0–0.08) alloys.

4. Conclusions

The discharge capacity of the BCC $Ti_{0.32}Cr_{0.43-x}Mn_xV_{0.25}$ alloys (x = 0–0.08) without ball-milling with the AB_5 alloy is much lower than the theoretical capacity. After ball-milling with the AB_5 alloy, the discharge capacity is improved significantly because particles of the AB_5 alloy on the surface of the alloys act as a path for hydrogen penetration. The discharge capacities of the Mn-substituted alloys are higher than that of the alloy without Mn. In particular, the $Ti_{0.32}Cr_{0.38}Mn_{0.05}V_{0.25}$ alloy delivers an excellent discharge capacity of 340 mAh g^{-1}. On the other hand, the cycle-life of the alloy is degraded by the substitution of Mn for Cr due to the lower Cr concentration. With the addition of Mn, the plateau pressure for hydrogen is lowered and the hydrogen-storage capacity of the alloy is increased, thereby facilitating surface activation of the electrode.

Acknowledgement

This research was supported by the Program for the Training of Graduate Students in Regional Innovation, which was conducted by the Ministry of Commerce Industry and Energy of the Korean Government.

References

[1] M.V. Ananth, M. Raju, K. Manimaran, G. Balachandran, L.M. Nair, J. Power Sources 167 (2007) 228–233.
[2] S. Shi, C. Ouyang, M. Lei, J. Power Sources 164 (2007) 911–915.
[3] M. Tliha, H. Mathlouthi, J. Lamloumi, A. Percheron-Guegan, J. Alloy Compd. 436 (2007) 221–225.
[4] J. Shi, F. Wu, D. Hu, S. Chen, L. Mao, G. Wang, J. Power Sources 161 (2006) 692–701.
[5] D. Lu, W. Li, S. Hu, F. Xiao, R. Tang, Int. J. Hydrogen Energy 31 (2006) 678–682.
[6] C. Wang, M. Marrero-Rivera, D.A. Serafini, J.H. Baricuatro, M.P. Soriaga, S. Srinivasan, Int. J. Hydrogen Energy 31 (2006) 603–611.
[7] C. Rongeat, M.-H. Grosjean, S. Ruggeri, M. Dehmas, S. Bourlot, S. Marcotte, L. Roué, J. Power Sources 158 (2006) 747–753.
[8] T. Ozaki, H.B. Yang, T. Iwaki, S. Tanase, T. Sakai, H. Fukunaga, N. Matsumoto, Y. Katayama, T. Tanaka, T. Kishimoto, J. Alloy Compd. 408–412 (2006) 294–300.
[9] R. Tang, X. Wei, Y. Liu, C. Zhu, J. Zhu, G. Yu, J. Power Sources 155 (2006) 456–460.
[10] E. Jankowska, M. Makowiecka, M. Jurczyk, J. Alloy Compd. 404–406 (2005) 691–693.
[11] F. Feng, D.O. Northwood, Int. J. Hydrogen Energy 30 (2005) 1367–1370.
[12] B. Huang, P. Shi, Z. Liang, M. Chen, Y. Guan, J. Alloy Compd. 394 (2005) 303–307.
[13] Y. Chai, M. Zhao, Int. J. Hydrogen Energy 30 (2005) 279–283.
[14] F. Zhang, Y. Luo, J. Chen, R. Yan, L. Kang, J. Chen, J. Power Sources 150 (2005) 247–254.
[15] H. Pan, X. Wu, M. Gao, N. Chen, Y. Yue, Y. Lei, Int. J. Hydrogen Energy 31 (2006) 517–523.
[16] Y. Zhu, H. Pan, M. Gao, J. Ma, Y. Lei, Q. Wang, Int. J. Hydrogen Energy 28 (2003) 311–316.
[17] S.W. Cho, G.C. Shim, G.S. Choi, C.N. Park, J.H. Yoo, J. Choi, J. Alloy Compd. 430 (2007) 136–141.

[18] S.W. Cho, C.N. Park, J.H. Yoo, J. Choi, J.S. Park, C.Y. Suh, G.S. Shim, J. Alloy Compd. 403 (2005) 262–266.
[19] S.W. Cho, C.S. Han, C.N. Park, E. Akiba, J. Alloy Compd. 289 (1999) 244–250.
[20] E. Akiba, H. Iba, Intermetallics 6 (1998) 461–470.
[21] X.B. Yu, Z. Wu, B.J. Xia, N.X. Xu, J. Alloy Compd. 386 (2005) 258–260.
[22] X.B. Yu, Z. Wu, B.J. Xia, N.X. Xu, J. Alloy Compd. 375 (2004) 221–223.
[23] M. Tsukahara, K. Takahashi, T. Mishima, T. Sakai, H. Miyamura, N. Kuriyama, I. Uehara, J. Alloy Compd. 226 (1995) 203–207.
[24] M. Tsukahara, K. Takahashi, T. Mishima, A. Isomura, T. Sakai, J. Alloy Compd. 253–254 (1997) 583–586.
[25] M. Tsukahara, T. Kamaiya, K. Takahashi, A. Kawabata, S. Sakurai, J. Shi, H.T. Takeshita, N. Kuriyama, T. Sakai, J. Electrochem. Soc. 147 (2000) 2941–2944.
[26] J.Y. Park, C.N. Park, C.J. Park, J. Choi, Int. J. Hydrogen Energy 32 (2007) 4215–4219.
[27] H.G. Moon, MS thesis, Chonnam National University, 2000.